Materials Advances

ROYAL SOCIETY OF CHEMISTRY

PAPER

View Article Online
View Journal

Cite this: DOI: 10.1039/d6ma00484a

Correlation-driven insulating behaviour in double perovskite ruthenate thin films A_2DyRuO_6 (A = Ba, Sr)

Jay Singh and Sahil Dani *

The structural, optical and electronic properties of double perovskite ruthenate thin films, specifically A_2DyRuO_6 (where A = Ba, Sr), have been thoroughly examined using various analytical methods. These methods include X-ray diffraction (XRD), UV-Vis spectroscopy, X-ray photoelectron spectroscopy (XPS), ultraviolet photoelectron spectroscopy (UPS), and X-ray absorption spectroscopy (XAS). XRD analysis of the films' structure shows the formation of highly crystalline, single-phase thin films with a preferred *c*-axis orientation. Furthermore, a contraction in the lattice and an increase in octahedral distortion are observed, which is attributed to the substitution of the larger Ba^{2+} ion with the smaller Sr^{2+} ion. Using UV-visible diffuse reflectance spectroscopy and the Kubelka–Munk method to analyze the results, we found that Ba_2DyRuO_6 and Sr_2DyRuO_6 have wide band gaps and behave like insulators, with optical band gaps of about 3.66 eV and 4.16 eV, respectively. XPS studies show that most of the ruthenium is in the Ru^{5+} oxidation state, with a small amount in the Ru^{4+} state. This suggests that there are mixed valence states that are probably caused by oxygen vacancies or local distortions. XAS measurements at the O K-edge show the unoccupied electronic states, and strong hybridization between Ru 4d and O 2p orbitals is shown by a clear pre-edge feature. Complementary UPS measurements investigate the occupied states, and the integrated UPS–XAS analysis demonstrates a distinct reduction of spectral weight at the Fermi level, thereby validating the insulating ground state in both compounds. The spectral features, such as the creation of lower and upper Hubbard bands, show that the insulating behavior is caused by electron–electron correlations in the Ru 4d manifold. Even though the structure changes when the A-site is replaced, both systems still show strong Mott–Hubbard insulating properties that are driven by correlation. This puts them close to the metal–insulator transition regime.

Received 7th April 2026,
Accepted 4th June 2026

DOI: 10.1039/d6ma00484a

rsc.li/materials-advances

1. Introduction

Transition metal oxides (TMOs) have been, and continue to be, a paradigm for the realization of novel quantum phenomena, where the interplay between charge, spin, orbital, and lattice degrees of freedom is subtle.[1–3] Specifically, the interplay between electron itineracy and electron–electron interaction leads to a variety of ground states, such as high-temperature superconductivity, colossal magnetoresistance, multiferroism, Mott insulating states, *etc.*[4–6] Among the aforementioned quantum phenomena, the Mott insulating state is at the heart of modern condensed matter physics because it violates the conventional band theory description of solids. In fact, according to band theory, partially filled energy bands in solids are expected to lead to metallic conductivity, whereas in Mott insulators, the presence of strong on-site Coulomb interaction leads to the localization of electrons in spite of the presence of partially filled energy bands, thereby exhibiting insulating behavior. Understanding and controlling such correlation-driven states remains one of the foremost challenges in modern materials physics.[7,8]

Ruthenium-based oxides are an interesting class of correlated materials because the Ru 4d orbitals are intermediate in spatial extension.[7,9–11] In comparison to the 3d-based systems, the Ru 4d orbitals are more spatially extended, and hence the bandwidth (W) is larger and the Coulomb repulsion (U) is generally smaller. However, in the right structure, the interplay between the two can yield a correlated insulating state. The ratio between the two energy scales depends sensitively on the crystal structure and the bond angles and lengths. Therefore, ruthenates are a suitable system in which the interplay between moderate electronic correlations and structural effects can be investigated.

Among complex oxides, the double perovskite $A_2BB'O_6$ has received much attention due to its structural flexibility and

TIET-VT Center of Excellence in Emerging Materials (CEEMS), Thapar Institute of Engineering & Technology, Patiala, Punjab 147004, India.
E-mail: sahildani22954@gmail.com

tunability.[12,13] In this perovskite structure, two different cations, B and B′, are located at alternating positions in the octahedral site, allowing the tailoring of the electronic and magnetic interactions.[14,15] The ordering of the structure, tolerance factor, and tilting of the octahedra are known to affect the electronic bandwidth and orbital overlap, thus controlling the level of correlation. In particular, if a 4d transition metal element, such as Ru, replaces a cation at the B-site, a variety of correlated electron states are possible.[16–20]

In the present study, we have chosen the double perovskite ruthenates A_2DyRuO_6, in which Ru occupies one of the octahedral sites and Dy occupies the other. By choosing Ba and Sr at the A site, we have the opportunity to study the influence of small changes in the lattice parameters and the octahedral distortion on the electronic structure. The difference in the ionic radii of Ba^{2+} and Sr^{2+} will result in a difference in the tolerance factor, thus changing the Ru–O–Ru bond angle and the bandwidth of the Ru 4d states. This will affect the strength of the electron–electron correlation and potentially the magnitude of the insulating gap. To understand the nature of the insulating state in these materials, there is a need for direct experimental access to the occupied as well as the unoccupied electronic states. XAS is used to study the unoccupied density of states. It is a powerful tool to study the hybridizations and the oxidation states of the relevant orbitals. In the case of Ru-based oxides, the relevant XAS edges are very sensitive to the degree of Ru 4d and O 2p hybridizations, which is very important for the determination of the bandwidth and the correlation strength.[21–23] Complementary to the information provided by XAS, XPS and UPS can be employed to gain insight into the occupied states. In XPS, the deeper core levels as well as the valence states can be analyzed to obtain information about the elemental composition and the chemical states. UPS, with its increased surface sensitivity and the capability to analyze the band structure with higher energy resolution near the Fermi level, can be employed to obtain information about the valence band structure and the existence or nonexistence of states at the Fermi level.

One of the most important features characterizing Mott–Hubbard insulators is the splitting of the d-band of the transition metal, giving way to the formation of the lower and upper Hubbard bands due to the strong interaction between electrons.[24–26] In this regard, it is possible to study this phenomenon by using spectroscopy, observing the presence of well-defined features in the occupied and unoccupied density of states, separated by a band gap due to the interaction effects. The spectral weight distribution and energy separation between these features can be directly examined through combined photoemission and absorption measurements. In this way, it is possible to estimate the band gap by aligning the occupied and unoccupied density of states, thereby establishing the origin of the band gap.[27–30]

The reported work is an extension of our previously published article based on the experimental and theoretical studies of the structural and magnetic properties of thin films of double perovskite ruthenates: Ba_2DyRuO_6 (BRDO) and Sr_2DyRuO_6 (SDRO).[9] This study seeks to answer the following fundamental questions: (i) what is the nature of the valence and conduction band states in the A_2DyRuO_6 thin films? (ii) Is the insulating state related to conventional band-structure effects or to strong correlations between electrons? (iii) How does the replacement of Ba with Sr influence the strength of correlations and electronic structure? Our systematic analysis of XAS, XPS, and UPS results reveals that BDRO and SDRO exhibit a highly stable Mott–Hubbard type insulating ground state at room temperature. The Ru 4d and O 2p orbital hybridization effect is very significant in determining the electronic configuration, but at the same time, the Coulomb interaction between the Ru 4d orbitals is very vital in creating the observed gap. The substitution of A-site cations subtly affects structural parameters and bandwidth, but the insulating character is well preserved in these compounds.

2. Experimental details

A 247 nm KrF excimer laser with flux ≈ 2 J cm^{-2} and a repetition rate of 6 Hz was employed in the pulsed laser deposition method to deposit BDRO and SDRO thin films of $\sim$100 nm thickness on an $SrTiO_3$ (STO) (100) substrate maintained at 750 °C. The partial pressure of oxygen was maintained at 0.1 and 0.2 mbar during the deposition of BDRO and SDRO thin films, respectively. Then, the thin films were cooled to room temperature while maintaining the partial pressure of the gases at the same values and a cooling rate of 2 °C min^{-1}. The target–substrate distance was maintained at 4.5 and 4.1 cm during the deposition of BDRO and SDRO thin films, respectively. The X-ray diffraction pattern of the deposited compounds was recorded using a PANalytical X'Pert Pro X-ray diffractometer in order to investigate the structural phase of the compounds synthesized in the present investigation. The UV-visible spectra of the compounds synthesized in the present investigation were recorded using an Analytik Jena Specord 250 PLUS spectrophotometer in IIT Ropar. XPS measurements were made using an X-ray source of Al Ka (1486.6 eV) and an Omicron energy analyzer (EA-125, Germany), and XPS measurements were performed on the beamline BL-01, Indus-2, RRCAT, Indore, India. The Ru M2,3 edge of the compounds synthesized in the present investigation was recorded using X-ray absorption spectroscopy in TEY mode. Before recording XAS and XPS spectra, the compound pellets were subjected to plasma treatment to generate fresh surfaces.

3. Results and discussion

3.1. Structural analysis

We used a PANalytical X'Pert Pro diffractometer to perform high-resolution X-ray diffraction (XRD) measurements on the A_2DyRuO_6 (A = Ba, Sr) thin films to determine their purity and crystallinity. The θ–2θ scans show that both BDRO and SDRO thin films grow in a single phase with a strong (004) reflection (as shown in Fig. 1). This means that the *c*-axis growth is very well oriented on the $SrTiO_3$ (STO) substrate. The lack of secondary impurity peaks within the instrument's detection

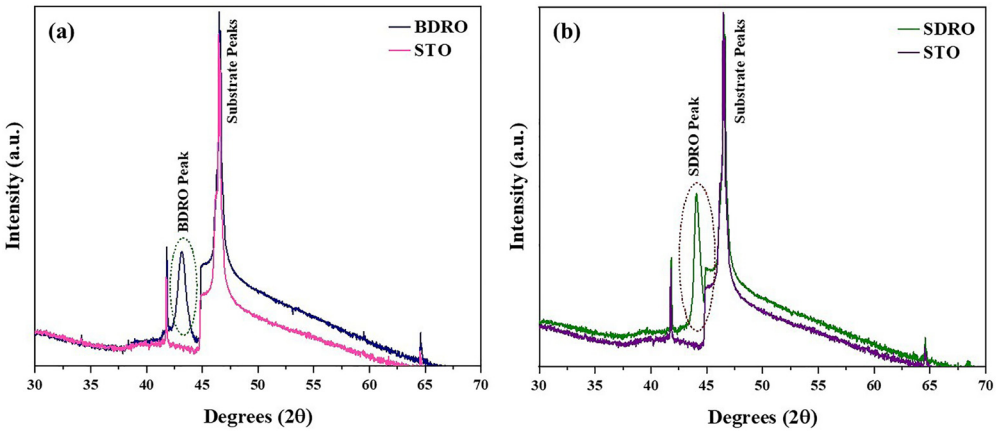

Fig. 1 θ–2θ XRD patterns of BDRO and SDRO thin films deposited on STO substrates, revealing their single-phase nature with highly *c*-axis-oriented (004) reflections. The peak of the SDRO thin film shifts to higher 2θ values compared to the peak of the BDRO thin film, reflecting a reduced lattice parameter due to lattice contraction in Sr-substituted films.

limit demonstrates the films' high structural quality, which is necessary for accurate spectroscopic studies of intrinsic electronic properties. The bulk structural parameters of BDRO indicate a cubic lattice ($a = b = c = 8.3604$ Å),[31] while the lattice parameters of the monoclinic lattice of SDRO are $a \approx 5.778$ Å, $b \approx 5.794$ Å, $c \approx 8.184$ Å, and $\beta \approx 90.18°$.[32] In the thin film, the out-of-plane lattice parameter is found to be approximately equal to the bulk lattice parameter *c*, which is approximately equal to 8.374 Å for BDRO and 8.217 Å for SDRO. This shows that the essential framework of the double perovskite lattice remains the same.

A comparison of the (004) peaks indicates that the most intense peak is slightly shifted to higher 2θ values in SDRO (at 44°) compared to BDRO (at 43°). Bragg's law states that the shift of the peaks to higher 2θ values is due to the reduction of the out-of-plane lattice spacing. This is supported by the smaller lattice parameter observed in SDRO ($c \approx 8.217$ Å) compared to BDRO ($c \approx 8.374$ Å). The reduction of the lattice parameter can be understood by considering the smaller ionic radius of Sr^{2+} (132 pm) compared to Ba^{2+} (149 pm), resulting in a reduction of the unit cell volume and an increase in octahedral tilting.

Although the main focus of the present work is on the electronic structure at the core level and the valence states, as investigated through XPS, UPS, and XAS, the structural analysis assumes a significant supporting role. In fact, the small difference between the lattice parameters of BDRO and SDRO structures has a direct bearing on the Ru–O–Ru bond angles and the Ru–O bond lengths, thereby affecting the electronic bandwidth (W) of the Ru 4d states. In fact, the Mott–Hubbard insulator nature arises from the interplay between the on-site Coulomb interaction (U) and the bandwidth. The change in the lattice dimension in SDRO is also expected to change the extent of Ru 4d and O 2p hybridization, which is then reflected through the spectral weight change observed through the XPS and XAS measurements. Thus, the XRD results not only confirm the structural quality and phase purity of the thin films but also provide a structural basis for the correlation-driven electronic behavior observed in spectroscopic measurements.

3.2. Ultraviolet-visible spectrometer

The optical absorption characteristics and the nature of the electronic transition of the BDRO and SDRO thin films were examined using UV-visible diffuse reflectance spectroscopy, which is essential for understanding their optoelectronic integration potential. To determine the electronic structure, the reflectance data were converted to the corresponding absorption coefficient using the widely accepted Kubelka–Munk (K–M) radiative transfer equation,[33] which is given by the expression: $F(R) = (1 - R)^2/2R$, where R is the absolute reflectance.

This is particularly effective in thin film and powder samples, where the scattering effects of the material are taken into consideration. As shown in Fig. 2, the relationship between the absorption coefficient and the incident photon energy ($h\nu$) was modelled using the relation given by $(F(R)\cdot h\nu)^n = B(h\nu - E_g)$, where B is the material-dependent constant and E_g is the optical band gap. As per the literature, Ru-based double perovskites exhibit a direct allowed transition, where $n = 2$ is considered.[34] The optical band gap (E_g) values were determined by extrapolating the linear region of the $(F(R)\cdot h\nu)^2$ *vs.* $h\nu$ plots to the energy axis, where the K–M function is essentially zero. The E_g value was determined to be 3.66 eV for the BDRO thin film and 4.16 eV for the SDRO thin film. This high E_g value is a definitive indicator of the insulating nature of the compounds. With regard to condensed matter physics, if the band gap is above 3.0 eV, the material is considered to be a wide band gap insulator or semiconductor material, where the valence band is fully occupied and the conduction band is empty at room temperature.

The observed wide band gap is in excellent agreement with the results of similar double perovskite structures that have been reported in the literature, which have high electrical resistivity and optical transparency in the visible spectrum. It is interesting to note that there is an increase in the gap from 3.66 eV in BDRO to 4.16 eV in SDRO, which can be attributed to a strong modulation of the electronic states due to the ionic radii and electronegativities of the B-site cations. Moreover, the

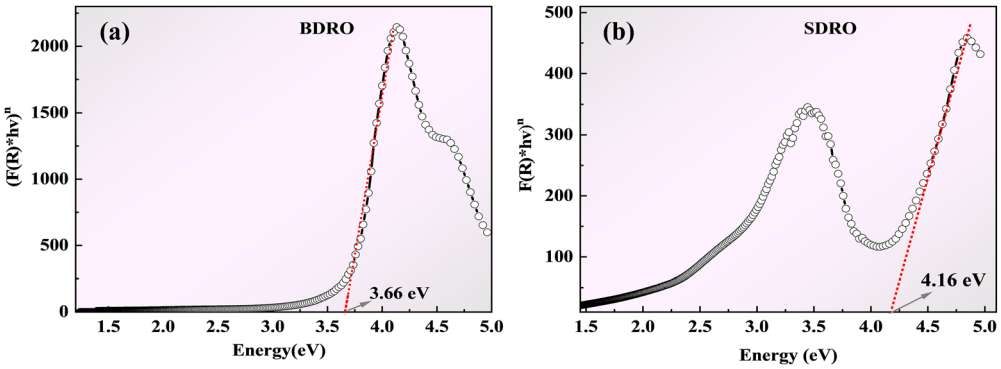

Fig. 2 Kubelka–Munk plots derived from UV-visible diffuse reflectance spectra of (a) BDRO and (b) SDRO thin films, illustrating direct allowed optical transitions.

steepness of the absorption edge in Fig. 2(a) also suggests a high quality of the films with few defects in the gap.

3.3. X-Ray photoelectron spectroscopy (XPS)

The X-ray photoelectron spectroscopy (XPS) spectra shown in Fig. 3(a–d) give detailed information about the Ru and O ion states and their electronic environment in the double perovskite thin films BDRO and SDRO. Panels (a) and (b) in the upper part of the figure show the Ru core-level XPS spectra, whereas the O 1s XPS spectra are shown in the lower part of the figure in panels (c) and (d) for BDRO and SDRO, respectively. The black line indicates the XPS spectrum, whereas the red line shows the overall envelope of the XPS spectrum after deconvolution. Additionally, the colored lines show the individual components of the XPS spectrum. The *x*-axis represents the binding energy, whereas the *y*-axis represents the intensity.

Fig. 3(a) and (b) show the Ru core-level XPS spectra of BDRO and SDRO compounds in the binding energy range of about

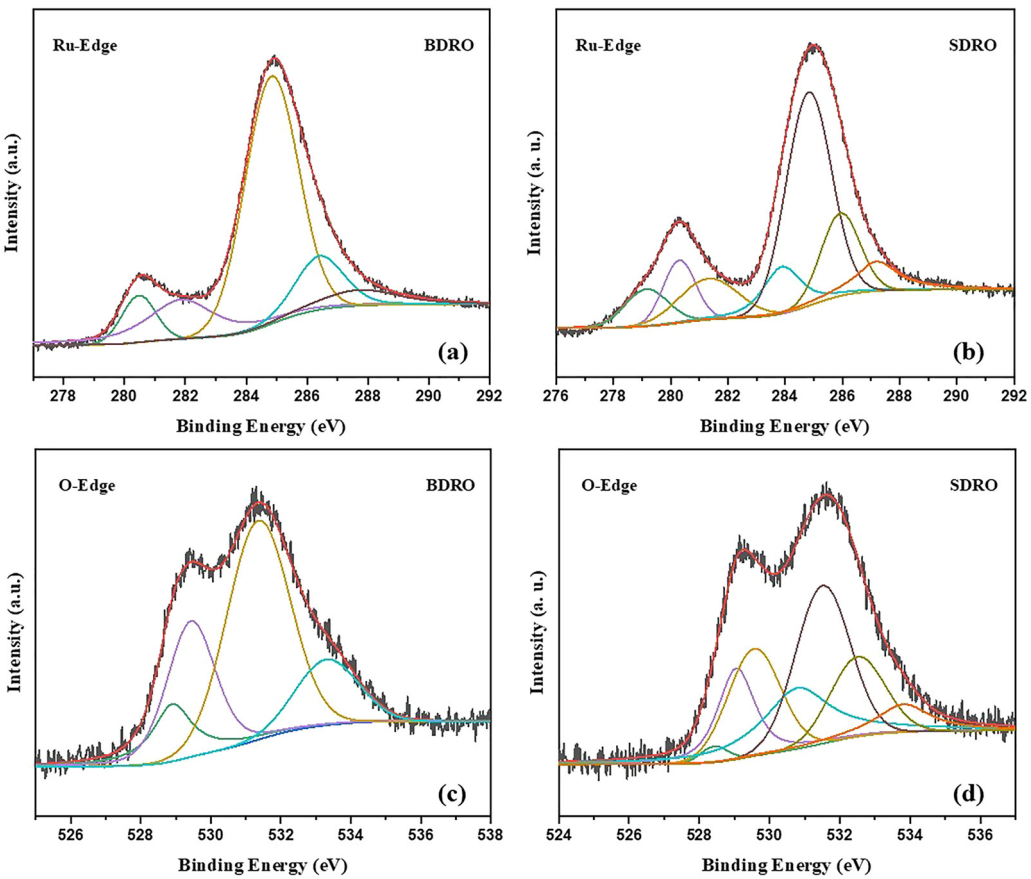

Fig. 3 XPS spectra of (a) and (b) Ru core-level and (c) and (d) O 1s for BDRO and SDRO thin films with fitted components. The spectra reveal dominant Ru^{5+} with minor Ru^{4+} states and contributions from lattice and defect-related oxygen.

276–292 eV. As seen, the Ru XPS spectrum has several features corresponding to the different Ru oxidation states. From the XPS spectrum, two main Ru oxidation states are seen in both compounds: Ru^{5+} and Ru^{4+}. From the Ru XPS spectrum of the BDRO thin film, the main peak at a binding energy of about 281.9 eV corresponds to the Ru^{5+} state, which is the expected Ru valence state in the stoichiometric double perovskite structure. This is attributed to the charge neutrality of the compound BDRO, in which Ba is present in the form of Ba^{2+}, Dy is present in the form of Dy^{3+}, and oxygen is present in the form of O^{2-}. The presence of Ru^{5+} also confirms that the Ru ion is present in the octahedral B-site of the perovskite structure in the RuO_6 coordination geometry. Apart from the peak of Ru^{5+}, there is also a peak present at ~280.5 eV, which is related to the presence of Ru^{4+} ions in the compound. The presence of the peak related to Ru^{4+} ions confirms that there is some contribution of reduced Ru ions in the compound, which might be present during the thin film deposition process.

Fig. 3(b) shows that the SDRO thin film also behaves in a similar manner. In addition, it can also be noted from the Ru core level spectrum that there are two states of oxidation present at the same time. In this case, it is evident that the Ru^{5+} ion is responsible for the main peak present at 281.3 eV. This indicates that the Ru ion is in its expected +5 valence state. There is a slight drop in binding energy compared to BDRO due to the change in the environment of the Ru ion. This is due to the fact that the crystal parameters of the materials have changed due to the replacement of Ba^{2+} with Sr^{2+} in the perovskite structure. Besides Ru^{5+}, a small peak appearing around ~280.3 eV corresponds to the Ru^{4+} state. The presence of Ru^{4+} confirms that there is a partial reduction of Ru^{5+}. This reduction may result from the presence of oxygen vacancies. The presence of Ru^{5+} and Ru^{4+} states confirms that there are mixed valence states, a common occurrence in metal oxides.

The quantitative analysis of the deconvoluted Ru core-level XPS spectra further provides insight into the relative concentration of Ru^{5+} and Ru^{4+} oxidation states in the BDRO and SDRO thin films. The integrated peak area analysis reveals that the relative percentage of Ru^{5+} is higher in the BDRO sample compared to the SDRO sample, whereas the contribution from Ru^{4+} is comparatively enhanced in SDRO. The obtained quantitative values are summarized in Table 1. The comparatively reduced Ru^{5+} concentration in SDRO can be attributed to the increased structural distortion associated with its monoclinic crystal structure. The monoclinic distortion modifies the local RuO_6 octahedral environment, resulting in enhanced lattice strain and a higher tendency for oxygen deficiency, thereby promoting the partial reduction of Ru^{5+} and Ru^{4+}. This observation is consistent with the comparatively larger oxygen vacancy concentration estimated from the O 1s spectra of SDRO. Therefore, the quantitative XPS analysis confirms that the crystal symmetry and local structural distortion strongly influence the Ru valence distribution in these double perovskite ruthenate thin films.

Table 1 Gaussian parameters, including peak positions, FWHM, and area, of the BDRO and SDRO compounds obtained from XPS spectra

	Position (eV)		FWHM (eV)		Area (eV)	
Compound	Ru^{5+}	Ru^{4+}	Ru^{5+}	Ru^{4+}	Ru^{5+}	Ru^{4+}
BDRO	281.3	280.4	1.29	0.855	1.7	1.3
SDRO	281.4	280.3	1.10	1.4	0.8	3.8

The presence of Ru^{5+} and Ru^{4+} states in both compounds indicates that mixed valence states are present in the film. However, the intensity of Ru^{5+} is higher than that of Ru^{4+}, which again supports that Ru is in the +5 state and is in accordance with the charge neutrality requirement for the double perovskite structure. The difference in the binding energies for Ru in BDRO and SDRO again indicates that substitution at the A-site affects the Ru ions. Fig. 3(c) and (d) display the O 1s XPS spectra of BDRO and SDRO, respectively. The O 1s XPS peak is normally composed of various peaks due to different kinds of oxygen environments in the material. For both compounds, three peaks are identified corresponding to lattice oxygen, defect-related species, and surface-adsorbed oxygen or hydroxyl groups. For the BDRO thin film (Fig. 3(c)), it is found that the peak with the highest intensity in the range of ~531–532 eV is due to lattice oxygen (O^{2-}) bonded with metal ions in the perovskite structure. These oxygen ions form RuO_6 octahedrons, which are building blocks of the double perovskite crystal lattice. A second peak is found with slightly lower binding energy in the range of ~529–530 eV. This is due to oxygen ions bonded with Ru ions, which is due to strong hybridization of Ru 4d and O 2p orbitals. A third peak with higher binding energy in the range of ~533–534 eV is due to surface oxygen species such as hydroxyl groups, adsorbed oxygen molecules, or oxygen vacancy states.

As shown in the O 1s spectrum of SDRO in Fig. 3(d), a very similar spectral profile is observed, proving that the fundamental coordination of the oxygen environment does not change after the substitution of Ba by Sr. The contribution of the lattice oxygen environment dominates the spectrum, proving that the structure of the films maintains the perovskite oxide environment. However, the relative intensity of the higher binding energy component appears to be somewhat enhanced, compared to that of BDRO, and this may be associated with the presence of adsorbed species or oxygen vacancy defects. This may be explained by the structural distortions that are expected for the Sr-based structure, as a result of the substitution of Sr^{2+} for Ba^{2+}, a smaller ion. The oxygen vacancy concentration was estimated from the ratio of the integrated area of the defect-related O 1s peak to the total O 1s peak area obtained from the fitted XPS spectra. Using this approach, the oxygen vacancy ratio was determined to be approximately 13% for the BDRO compound and 15.6% for the SDRO compound, indicating a comparatively higher oxygen-defect concentration in the SDRO sample.

A comparison of the XPS spectra of BDRO and SDRO indicates that the compounds have similar chemical characteristics to Ru predominantly in the +5 oxidation state. However, the presence of Ru^{4+} states in both compounds indicates that the compounds have mixed valence character. The mixed

valence character in the compounds may be due to the presence of oxygen vacancies. The small shift in the binding energy of the Ru^{5+} state in the compound BDRO at 281.9 eV and in the compound SDRO at 281.3 eV indicates that the substitution at the A-site changes the electronic environment of the Ru ions. The O 1s spectra indicate the presence of lattice oxygen, defect-related oxygen, and surface oxygen. The presence of more defect-related oxygen in the compound SDRO indicates that the substitution at the Sr site in the compound SDRO introduces additional lattice distortions and oxygen vacancy sites.

3.4. X-Ray absorption spectroscopy (XAS)

Fig. 4 displays the O K-edge XAS spectra of the double perovskite compounds BDRO and SDRO. The O K-edge XAS spectra are useful for studying the transition of O 1s core-level electrons to unoccupied states of the O 2p orbitals, as well as the hybridization of these states with the Ru 4d orbitals. Therefore, the spectra are useful for studying the unoccupied density of states and the hybridization of the Ru and O orbitals.

As seen in the spectra, the intensity of the XAS spectra is shown as a function of the photon energy. The spectra of BDRO and SDRO are shown in Fig. 4(a) and (b), respectively. The spectra of both compounds are similar, showing that the fundamental nature of the compounds' electronic structure is preserved. However, differences in the spectra are useful for studying the effects of A-site substitution on Ru–O hybridization.

Fig. 4(a) shows the O K-edge XAS spectrum of the BDRO compound, which exhibits a sharp and intense absorption peak at 532.3 eV. This is due to the pre-edge feature in the O K-edge XAS spectrum. The peak is due to the hybridization between O 2p and unoccupied Ru 4d states, particularly for t_{2g} states in RuO_6 octahedra. The pre-edge feature is commonly observed in transition metal oxide compounds due to the covalent interaction between O 2p and transition metal ions (Ru). The intensity of this peak is quite high, and it is attributed to Ru 4d and O 2p orbital hybridization. This is an important factor in determining the electronic states in compounds. The feature following the pre-edge is the broader feature in the region of 540–555 eV, which is related to the O 1s → hybridized O 2p and Ru 4d e_g levels, along with the Dy 5d levels. This is the conduction band feature of the material, which is related to the hybridization of the material. The gradual reduction in the absorption feature is related to the distribution of the unoccupied density of states related to the O and Ru ions.

Fig. 4(b) displays the O K-edge XAS spectrum of the SDRO compound. It can be noted that, similar to BDRO, the O K-edge XAS spectrum of SDRO displays a strong pre-edge peak at approximately 532.4 eV. This peak corresponds to the transition of the O 1s to O 2p hybridized Ru 4d states. The almost identical energy of the pre-edge peak in both compounds confirms that the local electronic environment of the Ru–O octahedral structure is maintained with the substitution of Ba with Sr. It can, however, be noted that there are some differences in the intensity of the spectral features of both compounds. The pre-edge peak of the SDRO compound appears sharper with a slight shift in energy compared to the BDRO compound. This shift in energy can be due to structural changes arising from the substitution of Ba^{2+} with the smaller Sr^{2+} ion. This substitution causes lattice contraction due to the smaller ionic radius of Sr compared to Ba, which affects the electronic states and hybridization in the RuO_6 octahedral network.

The structural changes also affect the Ru–O bond length and Ru–O–Dy bond angle, which in turn affect the overlap of Ru 4d and O 2p orbitals. Therefore, it is expected that the strength of hybridization and the character of unoccupied orbitals are slightly modified in SDRO compared to BDRO. In addition, in the higher energy range of 540–555 eV, it is found that the SDRO spectrum also contains a broad absorption band similar to that in BDRO. In this range of energy, transitions are allowed to the hybrid orbitals containing O 2p, Ru 4d e_g, and Dy 5d orbitals. Therefore, it is evident that this broad feature in the spectrum is due to extended hybridization in the perovskite structure.

3.5. Combined spectra

To determine the electronic structure of the BDRO and SDRO systems, the valence and conduction bands of the two

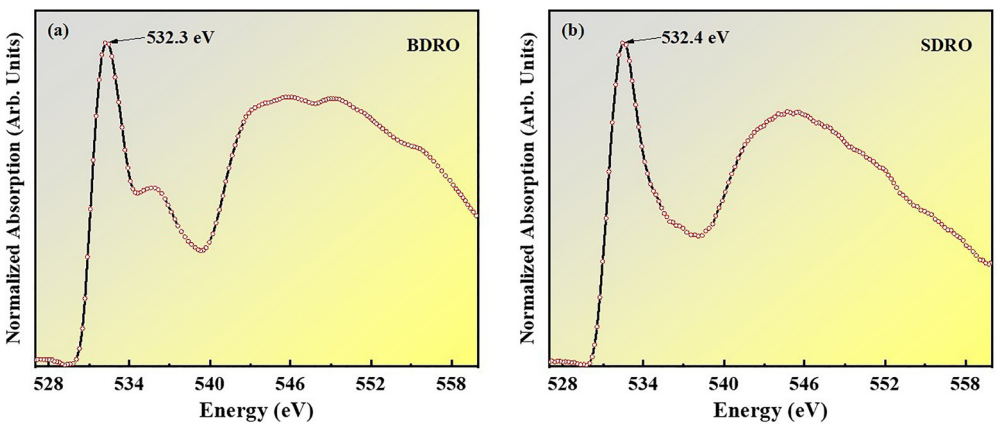

Fig. 4 Normalized O K-edge XAS spectra of (a) BDRO and (b) SDRO samples. The pre-edge peaks located at approximately 532.3 eV and 532.4 eV, respectively, correspond to the transitions from O 1s to the hybridized states of O 2p with transition metal d-orbitals. The broad features at higher energies represent transitions to higher-lying metal s, p, and O p states.

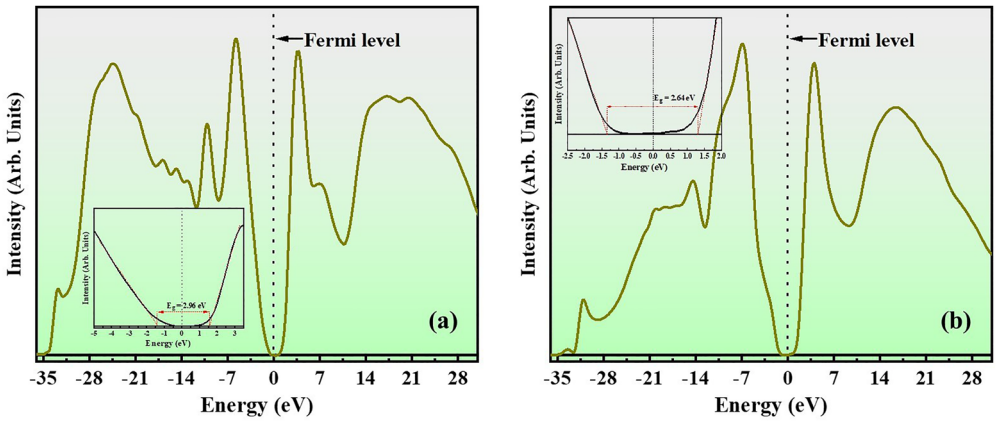

Fig. 5 Experimental density of states (DOS) for (a) BDRO and (b) SDRO determined by UPS and O K-edge XAS. The data show a clear energy gap centered at the Fermi level (E_F = 0), identifying both compounds as Mott insulators. Insets illustrate the band gap estimation (E_g), showing a narrowing of the gap from 2.96 eV in BDRO to 2.64 eV in SDRO.

compounds were combined in relation to the Fermi level. In order to form a plot that would contain information regarding both valence and conduction bands (O K-edge), the binding energy was plotted along the horizontal axis, while normalized intensity was plotted along the vertical axis (Fig. 5(a) and (b)). The valence band was acquired using ultraviolet photoelectron spectroscopy (UPS), which involves the study of the occupied states below the Fermi level.[7,35] The conduction band, on the other hand, is attained using XAS. The alignment of the spectra confirms that there is a suppression of states around E_F, proving that both compounds are insulators. The inset in the spectra shows the band edge region, from where the band gap of both compounds is estimated to be around ~2.96 eV for BDRO and ~2.64 eV for SDRO.

Another feature of the spectra is the presence of correlation-induced states, which are characteristic of strongly interacting electron systems. For the BDRO sample, the occupied states located around 5.7 eV are attributed to the lower Hubbard band (LHB), while the unoccupied states appearing near 3.7 eV in the conduction band region correspond to the upper Hubbard band (UHB). The observed electronic features are associated with the crystal-field-split t_{2g} and e_g states of the Ru (4d) manifold. Similarly, for the SDRO compound, the LHB is observed around 2.8 eV, whereas the UHB is located near 3.96 eV in the conduction band region, originating from the crystal-field-split Ru (4d) t_{2g} and e_g electronic states.

From the energy separation between the LHB and UHB, the on-site Coulomb interaction was estimated to be $U \approx 9.4$ eV for BDRO and $U \approx 6.7$ eV for SDRO, which is consistent with the values obtained from our reported DFT calculations.[9] The bandwidth for the Ru 4d-derived states is estimated to be in the range of 5–6 eV. This gives us an estimate of $U/W \approx 1.7$ for BDRO and 1.34 for SDRO. The U/W ratio for both compounds exceeds unity, indicating the presence of strong electron correlation and confirming their Mott insulating nature.

This indicates that both BDRO and SDRO are not normal band insulators but rather correlated insulators that lie close to the Mott transition boundary. This is because even with moderate levels of electron–electron interaction, there is always the formation of a gap with assistance from structural elements. The replacement of Ba with Sr, which is smaller in size, results in lattice contraction, thereby increasing the degree of distortion in the octahedra, which is equivalent to reducing the bandwidth W, moving closer to the Mott insulator. This is indicated by the reduced band gap in SDRO.

Importantly, the coexistence of Hubbard band features with a U/W ratio > 1 indicates that these compounds lie in a regime analogous to ruthenates near the metal–insulator transition, where electronic correlations and lattice effects cooperatively stabilize an insulating phase. The absence of a coherent quasiparticle peak at E_F, together with the clear LHB–UHB separation, strongly supports the classification of these materials as correlation-driven insulators in proximity to a Mott transition, rather than simple band insulators.

4. Conclusion

To summarize, in this study, we have successfully demonstrated the synthesis and comprehensive electronic characterization of high-quality, single-phase double perovskite ruthenate thin films, namely BDRO and SDRO, grown on $SrTiO_3$(100) substrates. From structural characterization using X-ray diffraction techniques, highly c-axis-oriented growth is confirmed, where lattice contraction is systemically achieved by replacing the larger Ba^{2+} (149 pm) with the smaller Sr^{2+} (132 pm) cation. More specifically, there is a decrease in the lattice parameter in the out-of-plane direction from 8.374 Å in BDRO to 8.217 Å in SDRO. The optical characterization of both materials using UV-visible diffuse reflectance spectroscopy classified both materials as having wide bandgap insulator properties with optical bandgap (E_g) values of 3.66 eV for BDRO, whereas that of SDRO was significantly modulated at 4.16 eV. Furthermore, using XPS, it was confirmed that ruthenium is predominantly in the +5 oxidation state, with characteristic peaks at ~281.9 eV in

BDRO and ∼281.3 eV in SDRO. The presence of a minor Ru^{4+} component also indicates possible minor oxygen deficiencies or structural distortions associated with the thin film growth process. O K-edge XAS measurements confirmed strong covalency between Ru 4d states and O 2p states, as indicated by a strong pre-edge feature at ∼532.3–532.4 eV. Most notably, UPS–XAS analysis confirmed the suppression of spectral weight at the Fermi level (E_F) with estimated electronic gap values of ∼2.96 eV for BDRO and ∼2.64 eV for SDRO. The lower Hubbard band (LHB) is identified at ∼−5.7 eV for BDRO and ∼−2.8 eV for SDRO, while the upper Hubbard band (UHB) features appear around ∼3.7 eV and ∼3.96 eV, respectively. From these features, the on-site Coulomb interaction was estimated to be $U \approx 9.4$ eV for BDRO and $U \approx 6.7$ eV for SDRO, with an estimated bandwidth of $W \approx$ 5–6 eV. The U/W values of ∼1.74 for BDRO and 1.34 for SDRO clearly indicate that these ruthenates exhibit Mott-insulating behavior: the electron–electron interactions, mediated by structural distortions, give rise to a robust Mott–Hubbard-type insulating state. The above results clearly indicate the robustness of the correlated state in complex oxide thin films and lay the basis for the integration of such materials in the emerging class of oxide electronics.

Conflicts of interest

There are no conflicts to declare.

Data availability

Data are available upon request from the authors.

Acknowledgements

We would like to thank TIET-VT Center of Excellence in Emerging Materials (CEEMS), Thapar Institute of Engineering & Technology, Patiala, Punjab, India for research infrastructure.

References

1 S. Okamoto, N. Mohanta, H. N. Lee, A. Moreo and E. Dagotto, *Phys. Rev. Materials*, 2025, **9**, 050301.
2 Y. Han, B. Lao, X. Zheng, S. Li, R.-W. Li and Z. Wang, *Front. Mater.*, 2024, **11**, 1444769.
3 Y. Li, J. Zhou and D. Wu, *ACS Appl. Mater. Interfaces*, 2019, **11**, 3565–3570.
4 N. Boora, R. Ahmad, S. Rahman, N. Q. Dung, A. Ahmad, M. B. Alshammari and B.-I. I. Lee, *Magnetochemistry*, 2025, **11**, 5.
5 M. An, Y. Weng, H. Zhang, Jun-J. Zhang, Y. Zhang and S. Dong, *Phys. Rev. B*, 2017, **96**, 235112.
6 Y. L. Wang, M. F. Liu, R. Liu, Y. L. Xie, X. Li, Z. B. Yan and J.-M. Liu, *Sci. Rep.*, 2016, **6**, 27840.
7 S. Dani, R. Pandit, A. Babu and R. Kumar, *J. Alloys Compd.*, 2024, **1006**, 176184.
8 F. Lechermann, *npj Comput. Mater.*, 2021, **7**, 120.
9 S. Dani, R. Kumar, H. Sharma, R. J. Choudhary, N. Goyal, P. Kaur and R. Pandit, *Phys. Chem. Chem. Phys.*, 2023, **25**, 20863–20870.
10 S. Dani, R. Pandit, H. Sharma, A. Arya, R. J. Choudhary, N. Goyal, J. Singh and R. Kumar, *J. Mater. Chem. C*, 2023, **11**, 4081–4093.
11 S. Dani, A. Arya, H. Sharma, R. Kumar, N. Goyal, R. Kumar and R. Pandit, *J. Alloys Compd.*, 2022, **913**, 165177.
12 M. Hjiri and N. Mustapha, *Mol. Catal.*, 2026, **595**, 115844.
13 L. Chen, J. Dinga and X. Zhu, *RSC Appl. Interfaces*, 2025, **2**, 320–351.
14 R. Yin, G. Yu, W.-Y. Cong, C. Guan, J. Li and Y.-B. Lu, *ACS Appl. Mater. Interfaces*, 2020, **12**, 44798–44804.
15 M. Z. M. Halizan, Z. Mohamed and A. K. Yahya, *Sci. Rep.*, 2021, **11**, 9744.
16 L. T. Nguyen, M. Saubanère, Q. Zhang and R. J. Cava, *Chem. Mater.*, 2021, **33**, 600–607.
17 E. K. Albrechta and A. J. Karttunen, *Dalton Trans.*, 2022, **51**, 16508–16516.
18 K. Naveen, T. Rom, S. S. Islam, M. Reehuis, P. Adler, C. Felser, A. Hoser, R. C. Nath, A. K. Yadav, S. N. Jha, D. Bhattacharyya, M. Schmidt and A. K. Paul, *Phys. Chem. Chem. Phys.*, 2021, **23**, 21769–21783.
19 T. Cui, T. Lin, Q. Jin, S. Chen, H. Hong, Q. Zhang, Y. Fan, D. Rong and J. Wang, *Phys. Rev. Mater.*, 2023, **7**, 115802.
20 J.-S. Zhou, C.-Q. Jin, Y.-W. Long, L.-X. Yang and J. B. Goodenough, *Phys. Rev. Lett.*, 2006, **96**, 046408.
21 E. B. Guedes, F. Abud, H. P. Martins, M. Abbate, R. F. Jardim and R. J. O. Mossanek, *Phys. Rev. B*, 2019, **100**, 075132.
22 W. T. Hong, K. A. Stoerzinger, B. Moritz, T. P. Devereaux, W. Yang and Y. Shao-Horn, *J. Phys. Chem. C*, 2015, **119**, 2063–2072.
23 C. A. Triana, D. A. Landínez Téllez and J. Roa-Rojas, *Mater. Charact.*, 2015, **99**, 128–141.
24 J. M. Kurdestany and S. Satpathy, *Phys. Rev. B*, 2017, **96**, 085132.
25 H. S. Lee, S. G. Choi, H.-H. Park and M. J. Rozenberg, *Sci. Rep.*, 2013, **3**, 1704.
26 J. Varignon, M. Bibes and A. Zunger, *Phys. Rev. B*, 2019, **100**, 035119.
27 J.-S. Kang, S. C. Wi, S. S. Lee, G. Kim, H. M. Yang, B. W. Lee, S. W. Han, K. H. Kim, A. Sekiyama and S. Kasai, *J. Phys.: Condens. Matter*, 2004, **16**, S5685.
28 G. Kim, S. S. Lee, H. J. Lee, J.-S. Kang, S. W. Han, J. Kim, B. W. Lee, H. G. Lee, J.-Y. Kim and B. I. Min, *J. Magn. Magn. Mater.*, 2007, **310**, 1969–1971.
29 J.-S. Kang, H. Han, B. W. Lee, C. G. Olson, S. W. Han, K. H. Kim, J. I. Jeong, J. H. Park and B. I. Min, *Phys. Rev. B: Condens. Matter Mater. Phys.*, 2001, **64**, 024429.
30 J.-S. Kang, J. H. Kim, A. Sekiyama, S. Kasai, S. Suga, S. W. Han, K. H. Kim, T. Muro and Y. Saitoh, *Phys. Rev. B: Condens. Matter Mater. Phys.*, 2002, **66**, 113105.

31 R. Kumar, C. V. Tomy, R. Nagarajan, P. L. Paulose and S. K. Malik, *Phys. B: Condens. Matter*, 2009, **404**, 2369–2373.
32 D. T. Adroja, S. Sharma, C. Ritter, A. D. Hillier, D. Le, C. V. Tomy, R. Singh, R. I. Smith, M. Koza, A. Sundaresan and S. Langridge, *Phys. Rev. B*, 2020, **101**, 094413.
33 P. Kubelka and F. Munk, *Adv. Electron. Mater.*, 1931, **12**, 593–599.
34 K. Kim, H. Kim and J. Park, *ACS Omega*, 2021, **6**, 26952–26958.
35 A. Jana, R. J. Choudhary and D. M. Phase, *Phys. Rev. B*, 2018, **98**, 075124.